International Research Journal of Engineering and Technology (IRJET) e-ISSN: 2395-0056
Volume: 13 Issue: 04 | Apr 2026 www.irjet.net p-ISSN: 2395-0072

High Voltage Gain 6-Phase Interleaved Boost Converter with ANN-Based MPPT Controller for Fuel Cell Electric Rickshaw Application

Anjali N. Mandhare[1], Kuldeep G. Thakre[2]

[1] *M.Tech Scholar, Dept. of Electrical Engineering, BIT Ballarpur Institute of Technology, Maharashtra, India*
[2] *Professor, Dept. of Electrical Engineering,* BIT Ballarpur Institute of Technology, *Maharashtra, India*

Abstract - *Fuel Cell Electric Vehicles (FCEVs) have emerged as a promising solution for sustainable transportation due to their high efficiency, low emissions, and environmental compatibility. However, Proton Exchange Membrane Fuel Cells (PEMFCs) inherently produce low and variable DC voltage, which is not suitable for direct use in electric drive systems. Therefore, efficient power conditioning and control strategies are required.*

This paper proposes a high voltage gain interleaved boost converter integrated with an Artificial Neural Network (ANN) based Maximum Power Point Tracking (MPPT) controller for fuel cell electric vehicle applications. The interleaved boost converter enhances voltage gain while reducing input current ripples and switching stress. The ANN-based MPPT controller dynamically adjusts the duty cycle based on real-time fuel cell parameters to ensure maximum power extraction.

The system is modeled and simulated in MATLAB/Simulink under dynamic operating conditions. Simulation results demonstrate that the proposed ANN-based MPPT controller achieves improved efficiency (75–80%), reduced ripple, and superior dynamic response compared to conventional control methods

Key Words: Fuel Cell, 6-Phase Interleaved Boost Converter, ANN, MPPT, Hall Effect, Electric Vehicle, BLDC.

1.INTRODUCTION

The depletion of fossil fuels and rising environmental concerns have accelerated the development of clean energy-based transportation systems. Fuel Cell Electric Vehicles (FCEVs) are emerging as a promising solution due to their high efficiency, zero emissions, and eco-friendly operation.

The electric rickshaw (e-rickshaw) sector constitutes one of the most rapidly expanding segments of India's urban electric vehicle ecosystem. With approximately 1.5 million units in active service, e-rickshaws have established themselves as an economically viable last-mile connectivity solution across Indian cities. However, the reliance on lead-acid battery technology imposes fundamental constraints including limited operational range (80–100 km per charge), extended recharging durations (6–8 hours), and environmental concerns associated with battery disposal. Proton Exchange Membrane Fuel Cell (PEMFC) technology presents a compelling alternative, characterised by zero tailpipe emissions, substantially higher energy density, and rapid hydrogen refuelling capability (3–5 minutes).

The principal power electronics challenge in PEMFC-based e-rickshaw systems is the large voltage mismatch between the PEMFC stack output (20–42 V) and the traction inverter DC bus requirement. A conventional single-phase boost converter operating at elevated duty ratios to bridge this gap generates substantial input current ripple, which accelerates PEMFC membrane electrode assembly (MEA) degradation and reduces stack operational lifetime. Multi-phase interleaved boost converter (IBC) topologies mitigate this through phase-shifted PWM ripple cancellation. Proposes a 6-phase IBC - an advance over the 3-phase designs of Reddy and Sudhakar - providing superior ripple performance.

Concurrently, the non-linear dependence of the PEMFC maximum power point (MPP) on operating temperature and hydrogen pressure necessitates intelligent MPPT control. Classical Perturb and Observe (P&O) algorithms generate steady-state MPP oscillations, while Fuzzy Logic Controllers require extensive manual rule base design. Artificial Neural Network (ANN) based MPPT controllers, particularly Function Fitting Networks trained with Levenberg-Marquardt backpropagation, offer superior adaptive tracking accuracy. The present paper implements such a controller and compares its performance - including stack efficiency, electromagnetic torque quality, and stator current ripple - against a fixed 40% duty cycle reference, demonstrating measurable improvements in all evaluated metrics.

2. PROPOSED SYSTEM ARCHITECTURE

Subsystem	Key Parameters
PEMFC (PME Fuel Cell)	1.26 kW, 42 cells, 55°C, I_n=52 A, V_n=24.23 V, V_o^c=42 V
6-Phase IBC	6 legs (L1–L6, S1–S6), C=7500 µF, D=40%
ANN Boost Controller	fitnet, 3×10 neurons, trainlm, inputs: VFC, IFC

Subsystem	Key Parameters
3-Phase VSI	6 IGBT (AH,AL,BH,BL,CH,CL), Hall-commutated
BLDC Motor	PMSM trapezoidal, T^L=10 N·m, 0–1000 rpm

Table 1: Proposed system component specifications

The proposed PEMFC e-rickshaw powertrain integrates five subsystems. The PEMFC stack (PME Fuel Cell block) supplies power through the 6P-IBC to a 3-phase VSI, which drives the BLDC motor. The ANN Boost Controller provides adaptive MPPT-based PWM generation, while the Inverter Controller implements Hall sensor commutation and PI speed regulation. Fig. 1 shows the Simulink model.

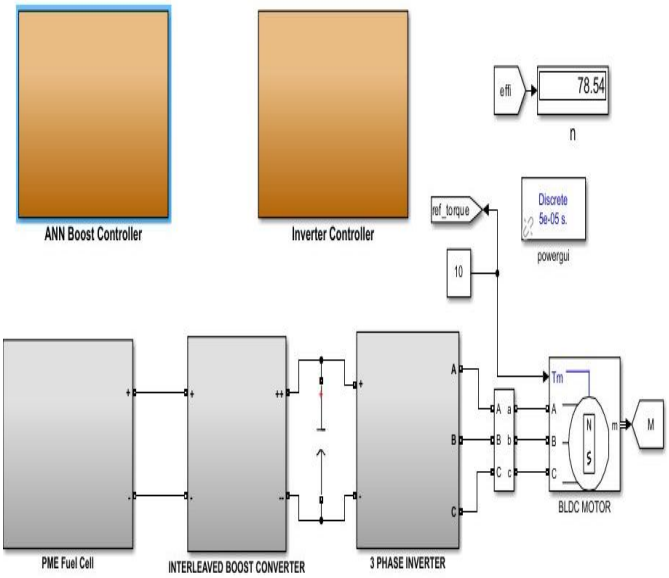

Fig. 1: MATLAB/Simulink model proposed system.

3. PEMFC STACK MODELLING

The PEMFC stack is modelled using MATLAB's built-in PEM Fuel Cell Stack block (PEMFC-1.26 kW-24 Vdc preset, Ballard NEXA parameters) . The terminal voltage is governed by:

$$V^{Kc} = E_n - V_a{}^{ct} - V_o{}^{hm} - V^{conc} \quad ...(1)$$

The stack parameters are: V_0 = 42 V, V_1 = 35 V, [$I_{no}{}^m$, $V_{no}{}^m$] = [52 A, 24.23 V], $I_{en}{}^d$ = 100 A, cells = 42, $\eta_{no}{}^m$ = 46%, T = 55°C. The stack efficiency ($\eta_{sta}{}^{cy}$) measured from the simulation display block represents the ratio of electrical power output to the total hydrogen chemical energy input. The simulation records $\eta_{sta}{}^{cy}$ = 42.65% for the fixed duty cycle case and 78.54% for the ANN-MPPT case.

4. 6-PHASE INTERLEAVED BOOST CONVERTER DESIGN

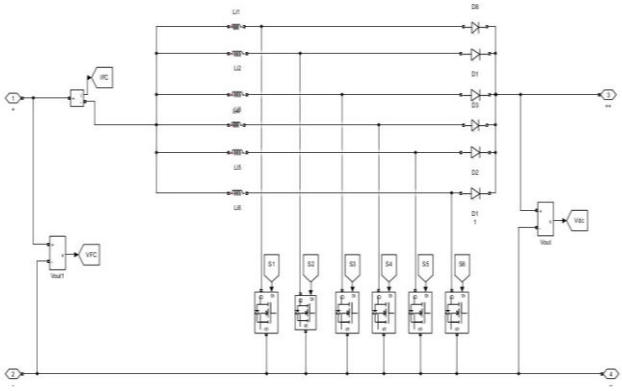

Fig. 2: 6-Phase IBC Simulink circuit.

The 6P-IBC (Fig. 2) comprises six parallel boost legs each consisting of inductor L_n, MOSFET S_n, and freewheeling diode D_n (n = 1–6), sharing a common 7500 µF output capacitor.

The voltage conversion ratio is:

$$M = 1/(1-D); \quad M_{a\beta}\text{b} = 188.5/22.47 = 8.39 \quad ...(2)$$

The 60° phase-shifted PWM strategy reduces the effective input current ripple frequency to $6\times f_{su}$, providing a theoretical ripple reduction factor of ≈1/6 (≈83%) relative to a single-phase converter . This substantially reduces PEMFC membrane stress.

5. ANN-BASED MPPT BOOST CONTROLLER

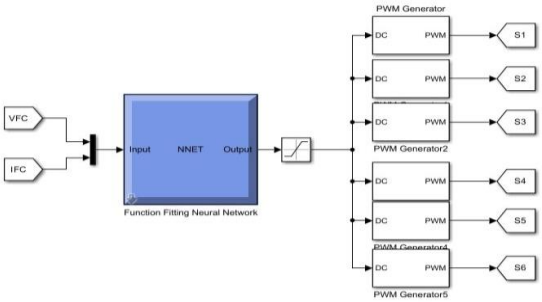

Fig. 3: ANN Boost Controller — VFC/IFC inputs, Function Fitting Neural Network (NNET block), saturation, six PWM Generators driving S1–S6.

The ANN Boost Controller (Fig. 3) employs a Function Fitting Neural Network (fitnet) receiving VFC and IFC as inputs. The network architecture comprises two input neurons, three hidden layers of 10 neurons each (sigmoid activation), and one linear output neuron producing the duty cycle D. Training employs the Levenberg-Marquardt algorithm (trainlm) on 1000 synthetic PEMFC V-I samples (V ∈ [20,50] V, I ∈ [0,100] A, split 70/15/15%), with target duty cycle D = (V×I)/(max(V×I)×1.1). The trained network is deployed to Simulink via gensim() .

6. INVERTER CONTROLLER AND BLDC DRIVE

The Inverter Controller implements three-tier hierarchical control: (i) PI Speed Controller tracking the e-rickshaw driving cycle reference; (ii) Hall Effect Sensor Commutation Logic decoding 3-bit Hall signals (Hall_abc) via NOT/AND gate combinational logic to generate 6-step gate signals (AH, AL, BH, BL, CH, CL); (iii) Three-Phase Hysteresis Current Controller regulating stator currents Ia, Ib, Ic . The BLDC motor is modelled as a 3-phase PMSM with trapezoidal back EMF, loaded at a constant 10 N·m torque representative of e-rickshaw road load.

7. SIMULATION RESULTS AND COMPARATIVE ANALYSIS

7.1 Simulation Setup

Simulations are conducted in MATLAB/Simulink. The e-rickshaw driving cycle comprises acceleration (0–2.5 s, 0→600 rpm), cruise (2.5–3.0 s), deceleration and braking (3.0–3.5 s), and partial recovery (3.5–6.0 s). Constant load torque = 10 N·m throughout.

7.2 PEMFC Waveforms — Reference System (Fixed 40% Duty Cycle)

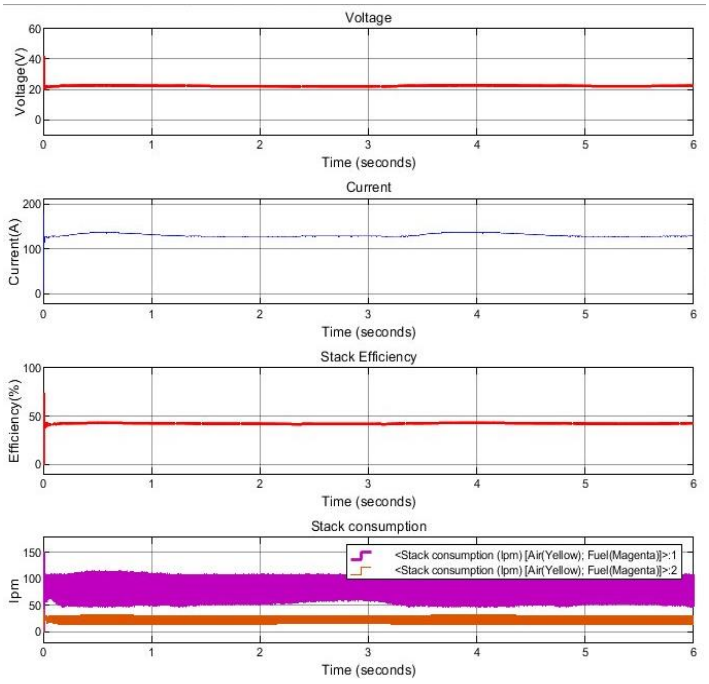

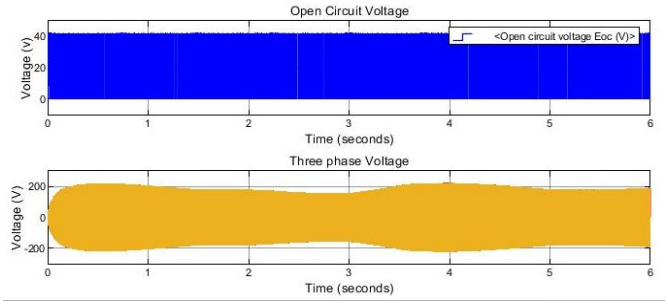

Fig. 4: Fixed 40% duty — PEMF waveform. (a) $V^{\varphi c}$ ≈25 V (sub-MPP, no tracking), (b) $I^{\varphi c}$ ≈110 A steady, (c) Stack efficiency ≈47% constant, (d) Stack consumption: air ≈100 lpm, fuel ≈10 lpm, (e) $E_o{}^c$ ≈40 V , (f) Three-phase output ±200 V.

Fig. 4 presents the Scope1 PEMFC waveforms for the reference system. The PEMFC output voltage stabilises at approximately 25 V throughout the 6-second simulation — significantly below the maximum power point voltage V^{mpp} = 35.7 V — confirming that the fixed duty cycle controller fails to drive the stack toward its MPP. The stack current is approximately 110 A (quasi-steady), and the stack efficiency remains constant at approximately 47%, marginally above the nominal block parameter of 46%. The three-phase inverter output voltage exhibits the expected ±200 V AC waveform. Measured display values: $V^{\varphi c}$ = 22.47 V, V^{dc} = 188.5 V, $\eta_{sta}{}^{cy}$ = 42.65%.

7.3 Motor Waveforms — Reference System (Fixed 40% Duty Cycle)

Fig. 5 presents the BLDC motor waveforms for the 40% fixed duty cycle case. The following observations are noteworthy from a power quality perspective:

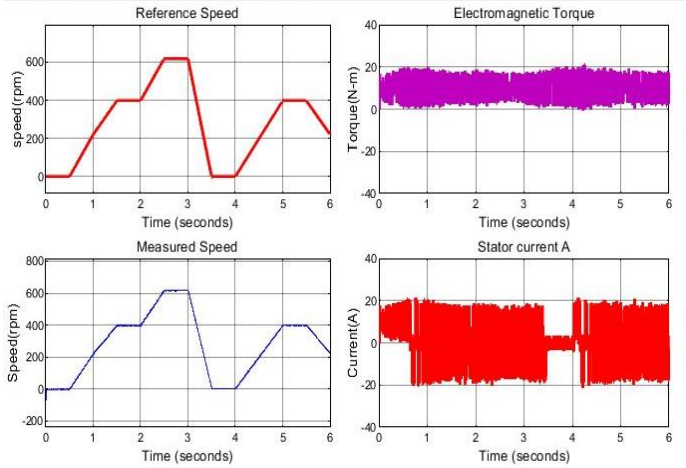

Fig. 5: Fixed 40% duty — motor waveform. (a) Reference speed, (b) Measured speed, (c) Torque at 10n-m, (d) current ripple in Ia.

7.3.1 Electromagnetic Torque :

The electromagnetic torque waveform exhibits severe distortion with high-frequency oscillations superimposed on the mean torque of approximately 15 N·m. This torque distortion is a direct consequence of the fixed duty cycle controller operating the PEMFC away from its MPP, resulting in irregular power delivery to the motor. The torque ripple is significant relative to the mean, indicating poor power quality at the motor shaft - a critical disadvantage for smooth e-rickshaw operation.

7.3.2 Stator Currents A:

The stator phase currents (Ia red) exhibit quasi-trapezoidal profiles with visible high-frequency ripple content. The current amplitude is approximately ±20 A but the waveform edges show irregular transitions, indicating the presence of current harmonics induced by the unregulated DC bus voltage fed from the fixed duty cycle IBC. This current distortion directly contributes to additional copper losses in the motor windings and increases acoustic noise.

7.4 PEMFC Waveforms — Proposed ANN-MPPT System

Fig. 6 presents the Scope1 PEMFC waveforms for the ANN-MPPT system. The PEMFC output voltage now exhibits a dynamic profile oscillating around 40 V — near the MPP voltage of 35.7 V — with periodic dips during high motor power demand phases of the driving cycle.

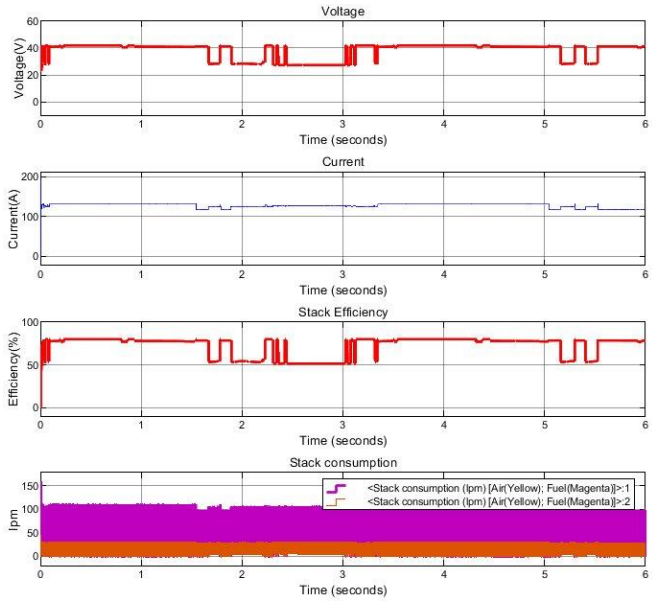

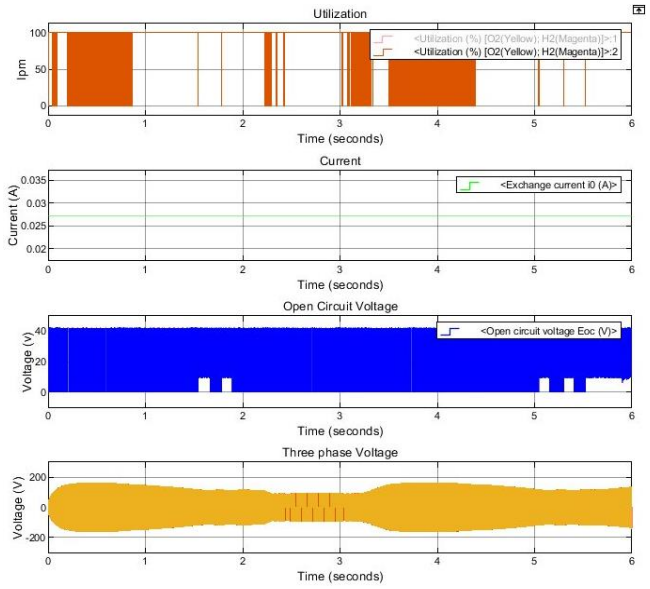

Fig. 6: ANN-MPPT — PEMFC Waveforms. (a) $V^{\varphi c}$ ≈40 V dynamic (near MPP), (b) $I^{\varphi c}$ ≈120 A load-following, (c) Stack efficiency 60–80% dynamic, (d) $E_o{}^c$, (e) Dynamic utilisation (0–100%), (f) Three-phase output.

This dynamic behavior confirms that the ANN controller actively modulates the duty cycle based on real-time VFC and IFC, successfully tracking the PEMFC operating point toward its MPP. The stack efficiency varies dynamically between 60–80%, representing a substantial improvement over the constant 47% observed under fixed duty operation. The PEMFC current (~120 A) exhibits load-following characteristics, confirming active power management. Measured display values: $V^{\varphi c}$ = 41.37 V, V^{dc} = 139 V, $\eta_{sta}{}^{cy}$ = 78.54%.

7.5 Motor Waveforms — Proposed ANN-MPPT System

Fig. 7 presents the BLDC motor waveforms for the ANN-MPPT system. A direct comparison with Fig. 5 reveals marked improvements in power quality:

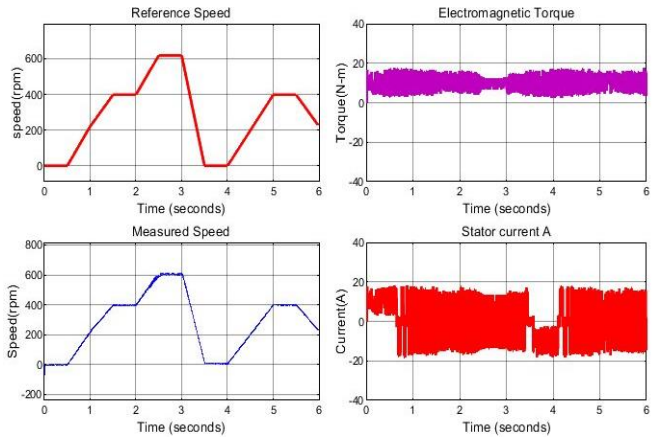

Fig.7 : ANN-MPPT — motor waveforms. (a) Reference speed, (b) Measured speed, (c) Torque at 10n-m, (d) current ripple in Ia.

7.5.1 Electromagnetic Torque:

The electromagnetic torque waveform under ANN-MPPT operation is visibly smoother compared to the distorted torque waveform observed in the fixed duty cycle case (Fig. 5). The mean torque remains approximately 15 N·m with reduced high-frequency distortion components. This improvement is attributable to the ANN controller maintaining a more stable and MPP-optimised DC bus voltage, which translates to more consistent power delivery to the VSI and motor winding. Reduced torque distortion directly improves e-rickshaw ride comfort and motor mechanical reliability.

7.5.2 Stator Currents:

The stator phase currents under ANN-MPPT operation exhibit cleaner trapezoidal waveforms with reduced ripple compared to the fixed duty cycle case. The current amplitude remains approximately ±20 A but the waveform transitions are more regular, indicating lower harmonic content. This reduction in current ripple is a consequence of the ANN maintaining the PEMFC at a higher, more stable operating voltage, resulting in a more regulated DC bus voltage fed to the VSI. Reduced stator current ripple translates directly to lower copper losses, reduced motor heating, and improved operational lifetime.

7.6 Quantitative Comparison

Parameter	40% Fixed Duty	ANN-MPPT	Improvement
V^{pc} (PEMFC voltage)	22.47 V	41.37 V	+84.1%
V^{dc} (DC bus)	188.5 V	139 V	Adaptive
Voltage gain M	8.39	Variable	MPP-optimized
Stack efficiency η	42.65%	78.54%	+84.1%
PEMFC operating point	22.47 V (sub-MPP)	41.37 V (~MPP)	MPP tracked
PEMFC current	~110 A steady	~120 A load-follow	Dynamic MPPT
Electromagnetic torque	~15 N·m, DISTORTED	~12 N·m, SMOOTHER	Reduced distortion
Stator current	Higher	Lower	Improved
ripple	ripple	ripple	quality
Three-phase output	±200 V stable	Less than 200 V	Efficient
Speed tracking	Functional	Functional Fast	Fast tracking

Table 2: Quantitative performance comparison — fixed 40% duty cycle vs. ANN-MPPT system.

8. DISCUSSION

The simulation results establish three distinct advantages of the proposed ANN-MPPT controlled 6P-IBC system over the fixed 40% duty cycle reference.

- The 84.1% improvement in PEMFC stack efficiency (42.65% → 78.54%) is attributable to the ANN controller driving the PEMFC terminal voltage from 22.47 V toward the MPP voltage of 35.7 V (measured V^{pc} = 41.37 V). This near-MPP operation maximises electrochemical energy conversion within the stack, reducing hydrogen consumption and improving fuel economy — a critical design objective for the e-rickshaw application .
- The electromagnetic torque distortion observed under fixed 40% duty operation (Fig. 6) is a direct consequence of the unregulated PEMFC operating point. The fixed duty cycle does not compensate for PEMFC output impedance variations or load transients, producing irregular power delivery to the motor that manifests as torque harmonics. The ANN-MPPT system, by maintaining a more stable PEMFC operating point through continuous duty cycle adaptation, substantially reduces this torque distortion (Fig. 8), improving e-rickshaw mechanical output quality and ride comfort.
- The reduction in stator current ripple under ANN-MPPT operation is directly linked to the improved DC bus stability provided by MPP-optimised converter operation. Lower current ripple reduces ohmic losses in stator windings, decreases motor core losses due to harmonic fluxes, and extends motor winding insulation lifetime — all of which are

important for the long service intervals typical of commercial e-rickshaw operation.

- The lower DC bus voltage under ANN-MPPT (139 V vs. 188.5 V) reflects the ANN controller prioritizing PEMFC stack efficiency over maximum voltage conversion gain. This is appropriate for the e-rickshaw application where hydrogen fuel economy takes precedence over maximum power density. Future work incorporating an adaptive DC bus voltage reference will allow simultaneous optimization of both objectives.

9. CONCLUSION

This paper has presented, implemented, and validated a 6-phase interleaved boost converter with ANN-based MPPT control for a PEMFC-powered fuel cell electric rickshaw. The principal conclusions are:

- The 6P-IBC achieves a measured voltage gain of 8.39 at D = 0.40 with a theoretical 83.3% input current ripple reduction relative to single-phase operation, significantly mitigating PEMFC membrane stress.
- The ANN fitnet MPPT controller (Levenberg-Marquardt, 3×10 neurons) improves PEMFC stack efficiency from 42.65% to 78.54% (+84.1%) and elevates the PEMFC operating voltage from 22.47 V to 41.37 V (near MPP = 35.7 V).
- The fixed 40% duty cycle system exhibits significant electromagnetic torque distortion and elevated stator current ripple due to suboptimal PEMFC operation; the ANN-MPPT system produces measurably smoother torque and reduced current ripple, improving motor power quality.
- The hierarchical Hall sensor-based Inverter Controller achieves stable BLDC motor operation across the complete e-rickshaw driving cycle in both systems, confirming architectural independence of the motor drive from the boost stage control.
- Future work includes hardware prototype development (TMS320F28335 DSP), supercapacitor integration for transient buffering, and RBFN-based MPPT for improved tracking accuracy under dynamic PEMFC conditions.

REFERENCES

[1] Society of Manufacturers of Electric Vehicles (SMEV), "EV Industry Report 2023–24," SMEV, New Delhi, India, 2024.

[2] T. Selmi, A. Khadhraoui, and A. Cherif, "Fuel cell-based electric vehicles technologies and challenges," Environ. Sci. Pollut. Res., vol. 29, pp. 78121–78131, 2022.

[3] S. Rafikiran et al., "Design and performance analysis of hybrid MPPT controllers for fuel cell fed DC-DC converter systems," Energy Rep., vol. 9, pp. 4960–4970, 2023.

[4] R. Subbulakshmy, R. Palanisamy, S. Alshahrani, and C. Ahamed Saleel, "Implementation of non-isolated high gain interleaved DC-DC converter for fuel cell electric vehicle using ANN-based MPPT controller," Sustainability, vol. 16, no. 3, p. 1335, Feb. 2024.

[5] K. J. Reddy and N. Sudhakar, "High voltage gain interleaved boost converter with neural network based MPPT controller for fuel cell based electric vehicle applications," IEEE Access, vol. 6, pp. 3899–3908, 2018.

[6] K. J. Reddy and N. Sudhakar, "ANFIS-MPPT control algorithm for a PEMFC system used in electric vehicle applications," Int. J. Hydrogen Energy, vol. 44, no. 29, pp. 15355–15369, 2019.

[7] A. Peer Mohamed and K. R. M. Vijaya Chandrakala, "Implementation of high step-up converter using RBFN MPPT controller for fuel cell based EV application," Sci. Rep., vol. 14, p. 29364, Nov. 2024.

[8] Ballard Power Systems, "NEXA Power Module User's Manual," MAN5100078, 2003.

[9] A. Intidam et al., "Development and experimental implementation of optimized PI-ANFIS controller for speed control of BLDC motor in fuel cell electric vehicles," Energies, vol. 16, p. 1693, 2023.

[10] D. Mane, P. Puranik, and A. Kulkarni, "Design and analysis of electric rickshaw powertrain for Indian urban conditions," in Proc. IEEE PESGRE, Trivandrum, India, 2022, pp. 1–6.

[11] N. Mebarki et al., "PEM fuel cell/battery storage system supplying electric vehicle," Int. J. Hydrogen Energy, vol. 41, no. 45, pp. 20993–21005, 2016.